ERRATA SHEET

Page 10, line 17

$C_p = \frac{p - p_\infty}{9_\infty}$, should read $C_p = \frac{p - p_\infty}{q_\infty}$

line 19

$\overline{C}_p = -\frac{2}{V_\infty}\frac{\partial \phi}{\partial t} - \frac{2\overline{u}}{V_\infty}$, should read $\overline{C}_p = -\frac{2}{V_\infty^2}\frac{\partial \phi}{\partial t} - \frac{2\overline{u}}{V_\infty}$

Page 13, line 42

20- x 30-ft should read 20- x 30-in.

WADC TN 55-64 March 1955

PRELIMINARY EXPERIMENTS ON THE SIMULATION OF GUSTS IN A WIND TUNNEL

A. M. Kuethe
J. D. Schetzer
L. C. Garby
R. L. Roensch

University of Michigan

Engineering Research Institute Project No. 2099-7-T
Contract No. AF 33(616)316
Project No. 53-670A-686 and 52-670A-86

United States Air Force
Wright Air Development Center
Air Research and Development Command
Wright-Patterson Air Force Base, Ohio

ABSTRACT

The report describes methods for generating reproducible gusts in a wind tunnel and tests conducted on an airfoil. The measured lift on the airfoil as a function of time is compared with theoretical predictions. The agreement is considered satisfactory for the scale of the tests conducted. A description is given of a larger scale gust-generator model now under construction.

OBJECTIVE

The objective of this constract is to study on a scale model and evaluate experimental techniques for the simulation of atmospheric gusts in a wind tunnel.

TABLE OF CONTENTS

LIST OF FIGURES

INTRODUCTION

The response of an aircraft to atmospheric gusts is of interest in structural design, in problems of riding comfort and guidance, and in the design of an aircraft as a launching or gun-firing platform. Since it is not feasible to determine the structure of a gust in the atmosphere except by the response of an aircraft to it, the simulation of atmospheric gusts in a wind tunnel is of special importance. Various methods of generating gusts have been considered, and the two most promising have been selected for development.

The development of devices for generating reproducible gusts in a wind tunnel is described in the following pages, along with the results of pilot model tests and comparison with theory. The associated instrumentation for measuring the effect of gusts on an aircraft, being an essential part of the development, is also described.

NATURE OF THE GUST SIMULATION PROBLEM

The end point of gust studies is the determination of aircraft response to the type of atmospheric turbulence likely to be encountered in flight. Two problems are posed, the first being the nature of atmospheric gusts, and the second, the response of an aircraft to these gusts. Actually, the two problems involve the same considerations, since the nature of atmospheric turbulence is deduced from the measured response of an aircraft that is flying through it.

Whether it is desired to predict the response of an aircraft to a known gust input as shown above or, alternatively, to determine the input from the measured response, the behavior of the aircraft in non-stationary flow must be understood. Ideally, gust-simulation studies should provide response information on an unconstrained elastic aircraft to unsteady flow of the same harmonic content as the atmospheric turbulence. The degree to which the designs that have been developed can be made to meet this criterion is discussed later.

APPLICATION OF A GUST MODEL TO DYNAMICS PROBLEM

The application of gust-simulation studies to the aircraft dynamics problem may be represented by the following block diagram:

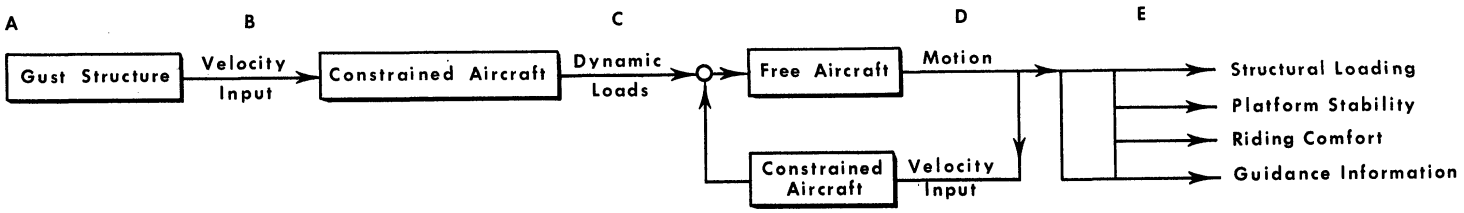

The gust structure is simulated by generating unsteady flows that have frequency spectra representative of those likely to be encountered in flight. Four major uses of data obtained from gust-simulation equipment are given below.

1. A major use of the experimental equipment is the measurement of dynamic loads produced on the constrained aircraft, as indicated by Section BC of the diagram above. Some aerodynamic configurations develop higher loads for a given gust input than do others; that is, their gust sensitivity is higher. The design problem of reducing gust sensitivity by proper aerodynamic shape (including gust alleviation devices) is aided by measurements on the constrained airplane.

2. A knowledge of the dynamic loads on the constrained aircraft is needed for a theoretical response analysis.

3. Aeroelastic problems can be studied by measuring the loads on an elastic model that is constrained as far as its free body motions are concerned.

4. The overall dynamics problem, which is essentially represented by sections B to D of the diagram, may be studied by releasing the constraints on the aircraft's degrees of freedom. It does not appear feasible to release all six constraints, however; this is unnecessary for many practical problems. For example, freedom in pitch alone is sufficient for the design of gust-load alleviation devices that sense the motion in pitch to obtain information for operating the alleviating mechanism. Platform stability in the longitudinal motions depend largely on pitch and plunge. Important characteristics at the stall are manifested by the rolling and yawing motions. Aeroelastic couplings with the rigid-body modes usually depend on fewer than six of the rigid-body degrees of freedom.

UNSTEADY AERODYNAMIC EFFECTS

If the flow field about an aircraft is changing rapidly, certain non-stationary effects come into play that make the lift and moment on the aircraft depart from their "quasi-steady" values. The term "quasi-steady" is used to denote the time-varying force that, at any instant, is equal to the steady state value corresponding to the flow configuration at that instant. The difference between the true dynamic lift and the quasi-steady value is called the lift lag.

The details of the various contributions to the lift lag is not understood for wing-body-tail combinations in which interference effects play a prominent role. For wings alone at subsonic speed, the lift lag is produced by the wake that accompanies the time-varying circulation and by the inertial reaction of the air to local acceleration. For simple plan forms, the so-called "wake lift" and apparent mass lift can be predicted from the theory of thin airfoils.

For a wing moving through a severe gust, the lift lag is known to be important. For a complete airplane with all interference effects considered, it is expected that the lift lag will also be a prominent factor. The lift lag is an essential feature of the gust problem, and therefore gust simulation equipment must include instrumentation that is adequate for the measurement of the lift lag.

Tests on the pilot model of gust-simulation equipment that are described in the following sections have been run on a constrained two-dimensional wing. The theory for this case is well understood and has served as a guide for developing the instrumentation necessary to measure the lift.

PREVIOUS WORK ON GUST SIMULATION AND RELATED PROBLEMS

In this section are cited typical references to literature on problems related to the dynamics of aircraft flying through gusts. No attempt is made to give a complete bibliography on the subject.

It is believed that the only facilities presently in use for simulating the effect of atmospheric gusts are of the NACA Langley Field type (References 1 and 2), in which a model is flown through an updraft of controlled profile and the resulting motion is observed photographically. The facility may be used to measure the re-
a velocity input B as shown on the diagram of page 2. Detailed informa-
-stationary aerodynamics (B to C) or airplane dynamics (C to D) taken
cannot be observed.

Experiments in unsteady aerodynamics have been confined very largely to the measurement of forces and moments on models that are oscillated in a wind tunnel. The frequency information so obtained is used for arbitrary periodic motions by applying the superposition principle. Experiments of this type have been reported in the literature as long as 20 years ago and they are currently being performed in ever-increasing numbers. Representative experiments on wings, bodies, and wing-body combinations are described in References 3 through 6.

Unsteady forces and moments have been calculated from the theory of thin airfoils for two- and three-dimensional wings moving through an incompressible fluid, and also for wings moving subsonically and supersonically through a compressible fluid. Numerical data appear in the literature in the form of the indicial admittance (response to a unit setup input) and the aerodynamic transfer function (response to a sinusoidal input). The response to an arbitrary input is found by Duhamel integration, using the indicial admittance, or Fourier synthesis, using the transfer function. Representative theory and calculations on non-stationary aerodynamics appear in References 7 through 16.

Among the earlier experiments on unsteady flow are those of Reference 17, in which an airfoil was set in motion in a water tank and the flow pattern made visible by shining light on suspended oil globules. The circulation build-up during the first few chords of airfoil travel was calculated from the motion of the globules. In Reference 18 direct force measurements were obtained on a wing near the stall, that was rotated at a rate of one degree in 2.5 chords of wing travel. In Reference 19 the author determined the circulation build-up on a wing by taking hot-wire measurements of the flow pattern around the tip-trailing vortices as the wing passed

through an updraft of known profile.

Calculations on the response of aircraft to gusts of given profile have appeared abundantly in the literature. A complete investigation requires that the rigid and elastic degrees of freedom of the aircraft be considered in investigating the response as the craft penetrates gusts of various sharpness. Though there is no difficulty in principle in assuming many degrees of freedom, the computational labor is large and most investigators have considered only a small number. Typical examples of these calculations are given in Reference 20, in which the authors have calculated the response of a rigid airplane to gusts of various degrees of sharpness, considering the plunging degree of freedom only.

Calculations have been made using both steady and unsteady flow theory. In Reference 21, the response of an airplane entering a sinusoidal gust, with the plunging and wing-bending degrees of freedom considered, has been calculated. Calculations on the influence of unsteady flow and structural flexibility on the rigid-body oscillations of an aircraft are numerous; typical examples are given in References 22 through 25. A general treatment of dynamics calculations is given in Reference 26. Finally, the nature of atmospheric turbulence, as deduced from meteorological measurements or the response of an airplane, is reported in the literature and typical examples are given in References 27 through 31.

METHODS AND APPARATUS FOR PILOT MODEL TESTS

There appears to be no standard for gust structure in the atmosphere. For that reason, the emphasis in this investigation has been to generate in the tunnel airstream reproducible disturbances of sufficient severity so that the wake and apparent mass effects are large enough to enable their accurate determination experimentally. Since, within the framework of thin-wing theory, these effects may be superimposed, it will be possible to obtain the response to a range of gust structures from representative tests.

The possible experimental techniques for measuring gust effects may involve the motion of a model through a disturbance (Reference 19) or the generation of a disturbance which sweeps over the model. The "moving model" technique appears to be more difficult and more expensive than the "fixed model" method, if representative Reynolds' numbers are to be attained. The fixed-model method was therefore chosen and various methods for generating reproducible gusts in a wind tunnel have been considered; two of the methods have been investigated experimentally in some detail.

The methods considered are of two types: a transient change in the boundary conditions at the wall of the wind tunnel in which the model is mounted, and the movement past the model of a disturbance generated upstream. Either method can be utilized to cause a disturbance to sweep over the model; the speed at which the disturbance moves is the speed of penetration of the model into the gust.

The first method developed for simulating a gust in the wind tunnel utilizes a moving bump, as shown schematically in Fig. 1. The curved streamlines upstream of the bump form a non-uniform flow field. The bump is moved downstream at speeds low

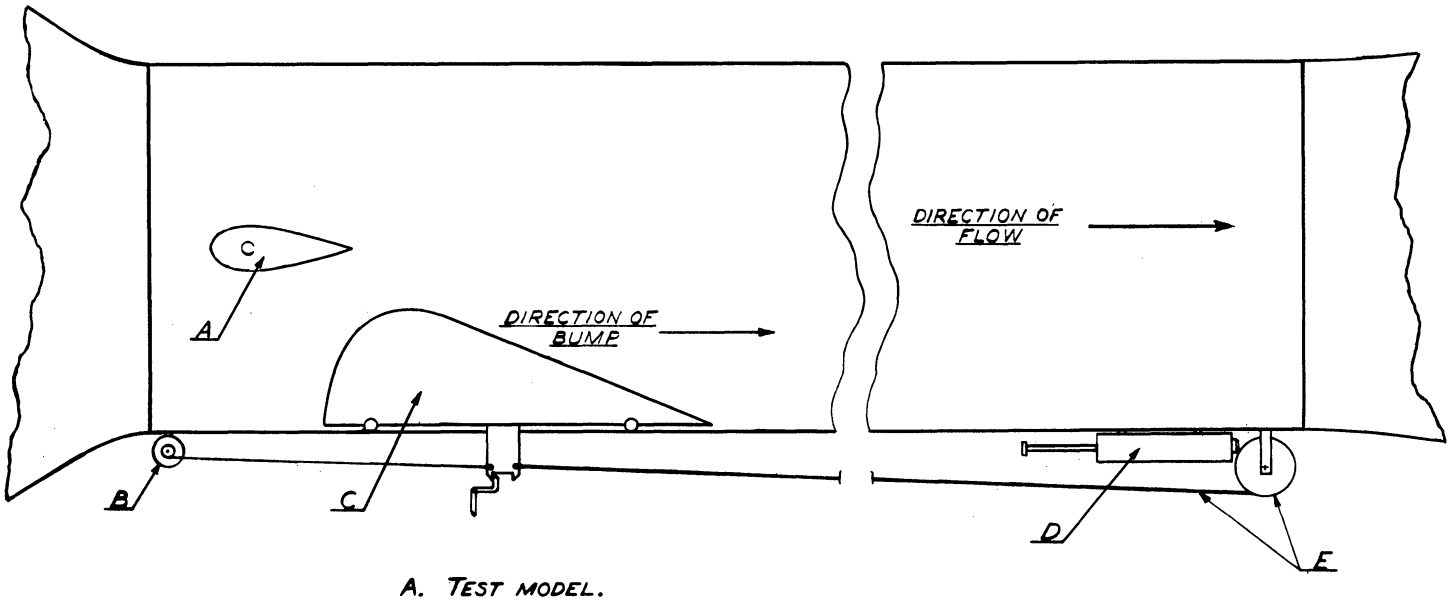

A. TEST MODEL.
B. POTENTIOMETER TO DETERMINE POSITION OF BUMP.
C. MOVING BUMP.
D. SHOCK ABSORBING CYLINDER.
E. ACCELERATING MECHANISM (AIRCRAFT SHOCK CORD & WINDING DRUM).

Fig. 1. Schematic diagram of moving-bump gust generator (See Fig. 2 of Progress Report No. 1).

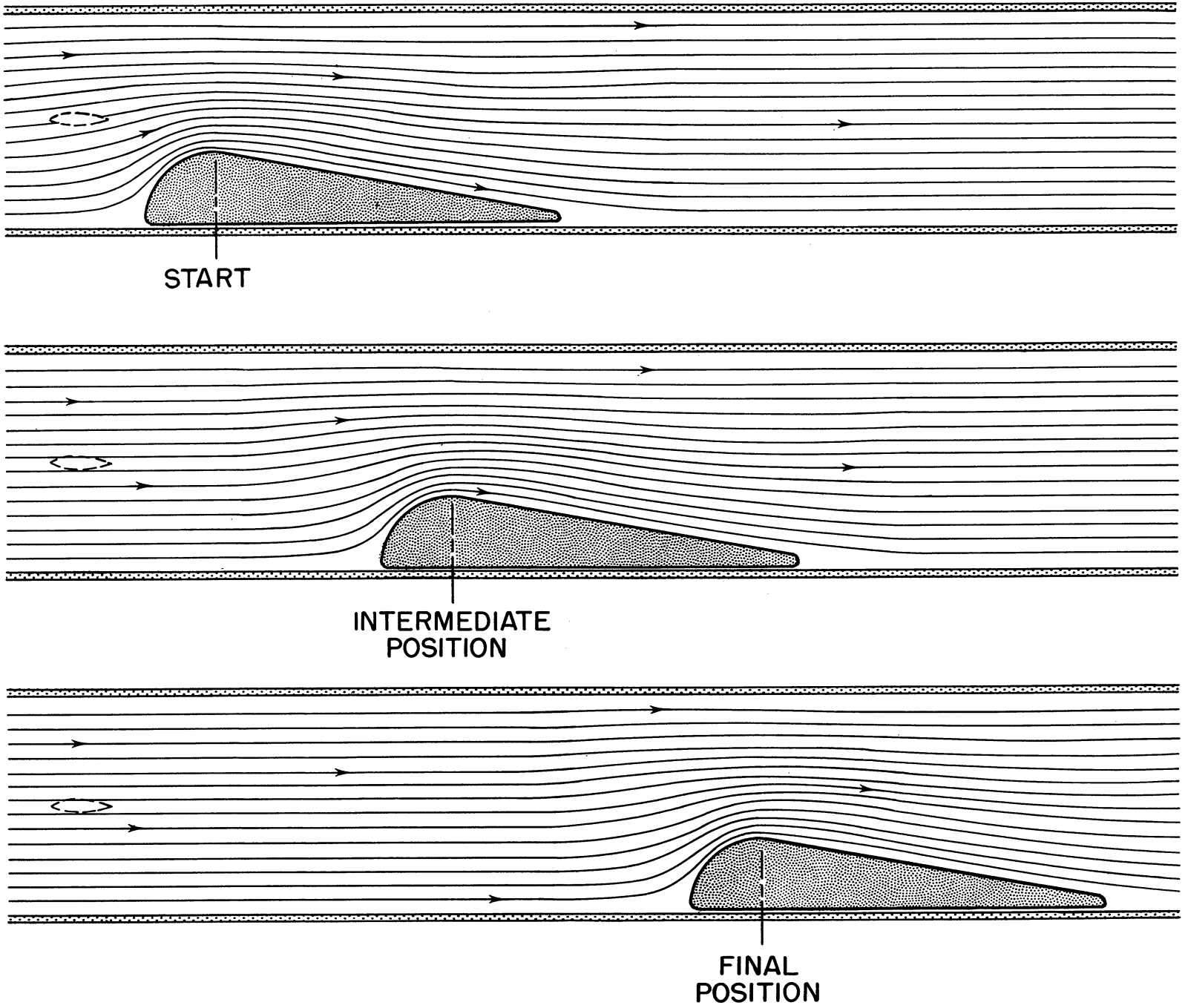

Fig. 2. Influence of bump upon flow field.

enough for the non-uniform field to follow it with no appreciable lag. As a result, the test model at point A experiences a varying flow field directly related to the position of the bump and the speed of the bump relative to the wind. The first order effect on the test model arises from the velocity component normal to the general direction of the flow. This is shown in Fig. 2 for three positions of the bump. Thus, as the bump moves downstream a gust-like pattern passes over the airfoil. The gust gradient is controlled by varying the ratio of the bump speed to the tunnel speed.

The second method for simulating a gust makes use of a "venetian blind" arrangement to generate a series of vortices that are carried downstream with the wind. The principle is illustrated schematically in Fig. 3. The "flippers" are given a positive angle of attack of 12° and then returned to neutral. If the motion is carried out rapidly, fairly discrete vortices are formed in pairs. Because the vortex pairs move downstream with the wind, their induced field forms a moving gust-like pattern. Due to the finite spacing and the viscous wake behind each of the vanes, it is difficult to obtain a uniform disturbance over the cross-section of the tunnel. However, it is easier to obtain very intense and rapid disturbances by this method than by the moving-bump method.

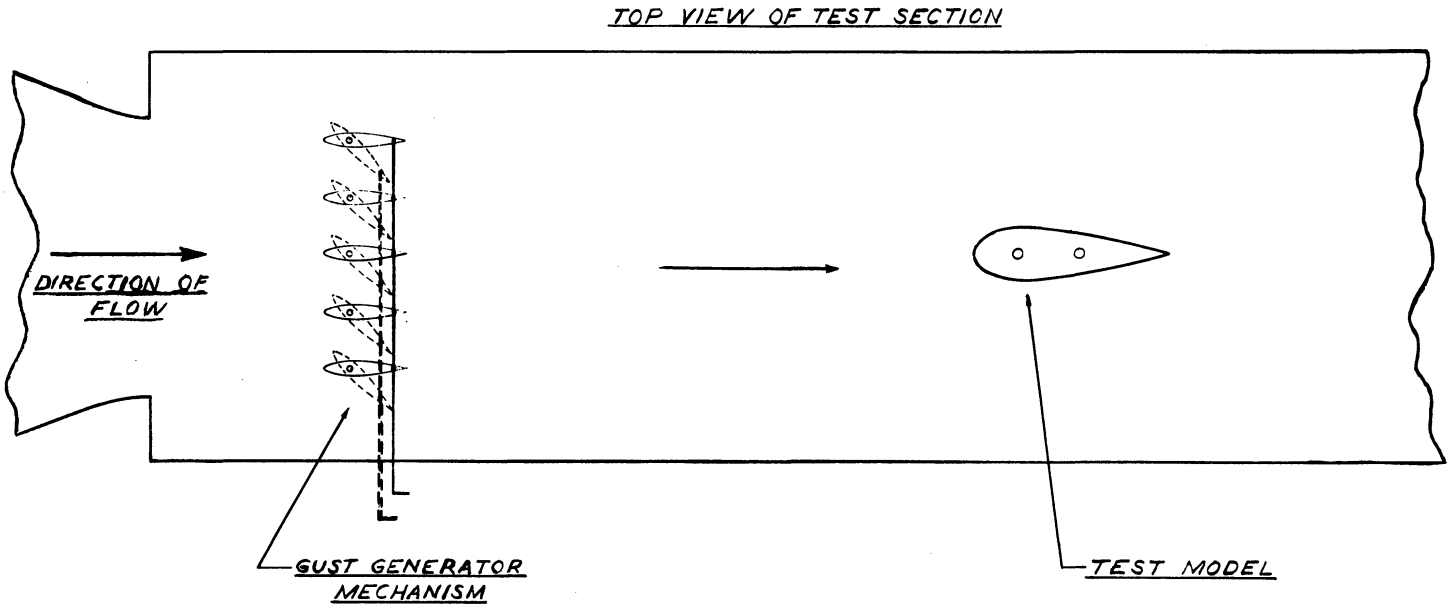

Fig. 3. Schematic diagram of vortex-type gust generator (Fig. 1 of Progress Report No. 1).

A small closed return-type tunnel generally used for instructional purposes was modified for the moving-bump program. A sketch of the circuit used is shown in Fig. 4. The circuit was opened in order to reduce the turbulence level caused by flow separation in portions of the return leg. Other methods for applying this method might involve downstream motion of a source or sink or through the use of inflatable inserts. Descriptions of the mechanical and instrumentation aspects of this system are given in References 32, 33, and 34.

For the vortex generator tests, rather extensive modifications were made to this circuit. A sketch of the circuit is shown in Fig. 5. With this circuit a turbulence level of 0.2% for $\overline{u}/U$ was obtained. Descriptions of the mechanical and instrumentative details are given in References 33, 35, and 36.

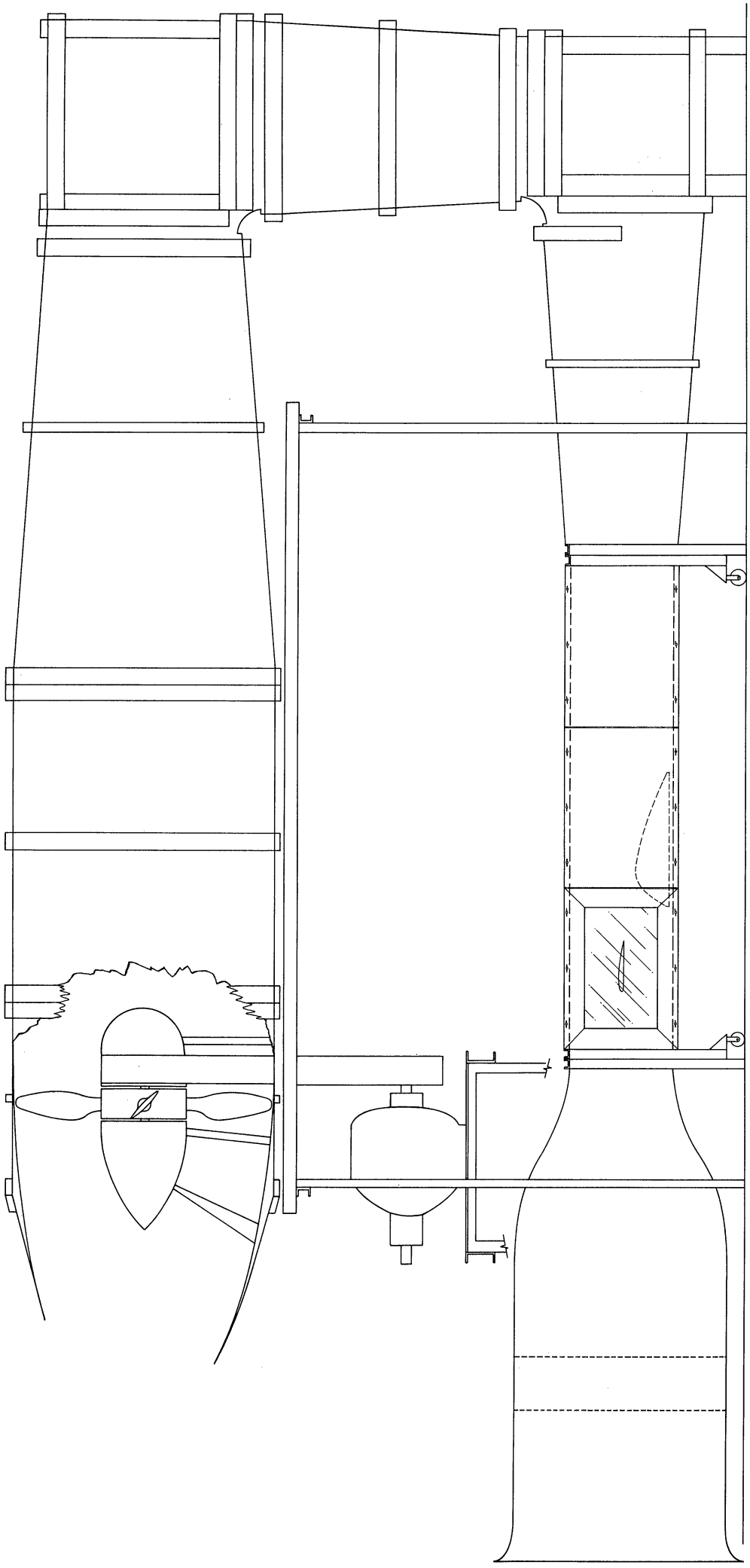

Fig. 4. Tunnel circuit used in moving-bump tests.

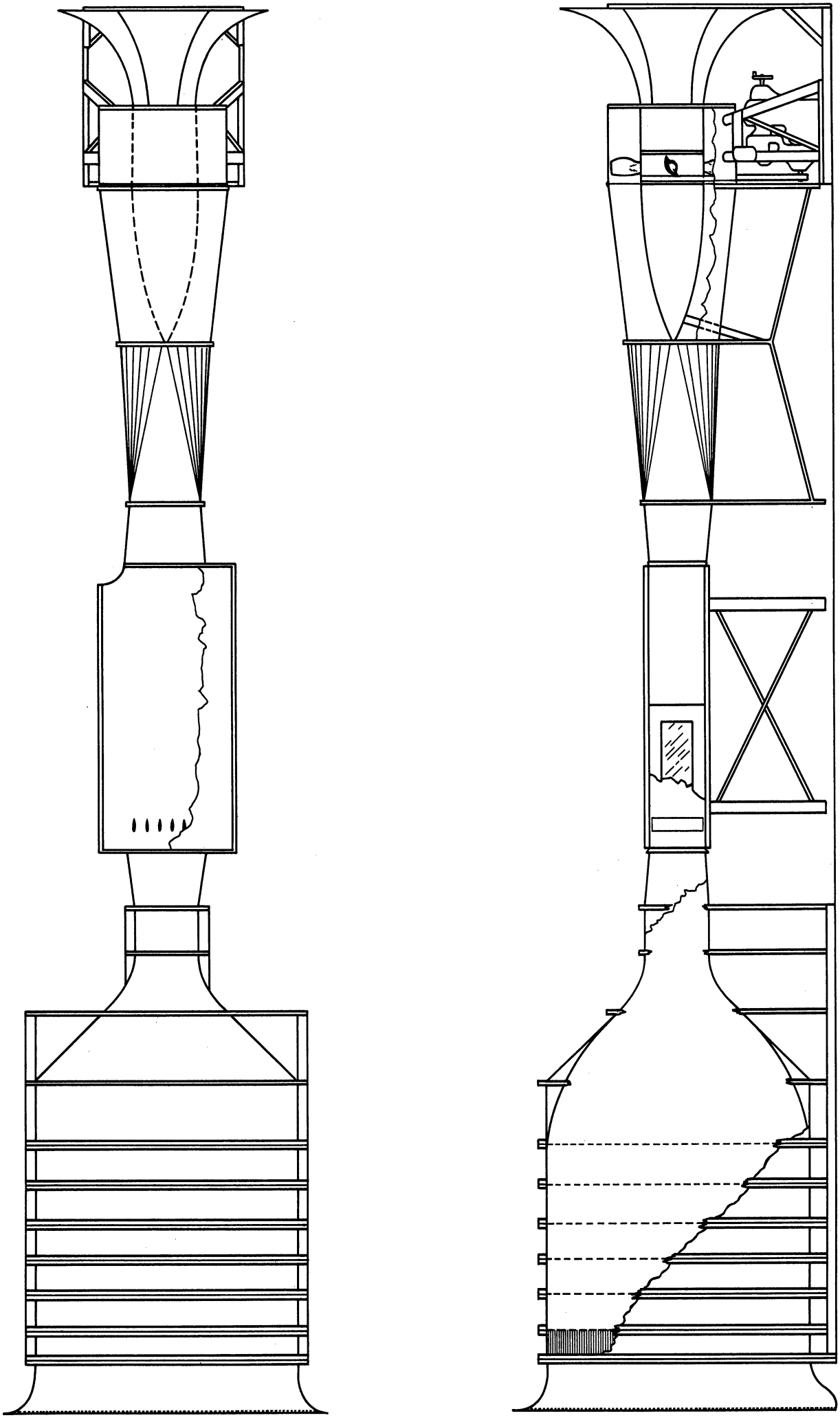

Fig. 5. Tunnel circuit employed with vortex-type gust generator.

RESULTS OF PILOT MODEL TESTS AND COMPARISON WITH THEORY

The effectiveness of the gust-generating devices were appraised by measuring the dynamic lift on a two-dimensional wing and comparing the test data with theory. In the following section, aerodynamic lift-lag theory for two-dimensional wings is briefly outlined. This is followed by samples of the measured data, using pilot models of the two devices.

AERODYNAMIC LIFT-LAG THEORY

Kinematically, the unsteady flow field is determined by Laplace's equation, $\nabla^2\phi = 0$, as in the steady flow case. The only difference is in the boundary conditions, which are functions of time for unsteady flow.

Dynamically, the pressure distributions on a model are determined by Euler's equation,

$$\rho\frac{DV}{Dt} + \text{grad } P = 0,$$

which for incompressible irrotational flow may be written

$$\nabla\left\{\frac{\partial\phi}{\partial t} + \frac{V^2}{2} + \frac{p}{\rho}\right\} = 0$$

or

$$\frac{\partial\phi}{\partial t} + \frac{V^2}{2} + \frac{p}{\rho} = H \ .$$

Linearizing in the usual fashion and forming the pressure coefficient $C_p = \frac{p - p_\infty}{q_\infty}$, we get

$$\overline{C}_p = -\frac{2}{V_\infty}\frac{\partial\overline{\phi}}{\partial t} - \frac{2\overline{u}}{V_\infty} \ ,$$

where the bar indicates surface values. For a two-dimensional thin airfoil in unsteady motion, the Kutta and Helmholtz conditions lead to the picture shown in Fig. 6.

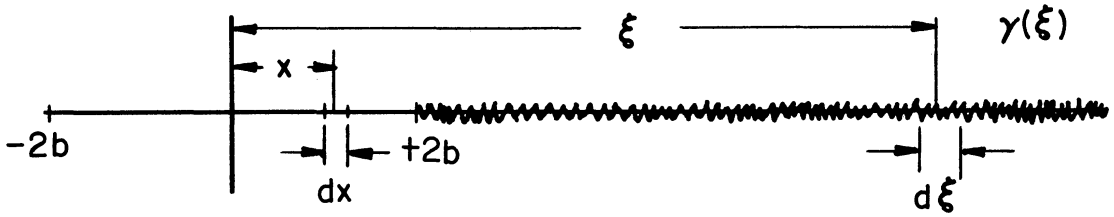

Fig. 6. Sketch of wake pattern behind airfoil.

The airfoil of chord 4b is followed by a wake of strength $\gamma(\xi)$. The surface velocity $\overline{u}$ and potential $\overline{\phi}$ that appear in $\overline{C}_p$ above include the wake effect.

Integrating $\overline{C}_p$ over upper and lower surfaces of the airfoil leads to the linearized expression for lift.

$$L' = -\rho \int_{-2b}^{+2b} \frac{\partial}{\partial t}(\overline{\phi_\ell - \phi_u})dx + \rho V_\infty (\Gamma_Q + \Gamma_w)$$

Γ_Q is the circulation about the airfoil ignoring the wake (quasi-steady) and Γ_w is the circulation arising from the velocity induced by the wake.

The physical interpretation of the first term is not clear because $(\phi_\ell - \phi_u)$ includes the potential induced by the wake, the potential associated with the circulation, and the potential of the acyclic flow. The integral, using only the acyclic potential, is the "apparent mass" effect. If the part of the integral not associated with the "apparent mass" is separated out and combined with $\rho V_\infty \Gamma_w$ (a process requiring about 10 steps), and if in addition Γ_w is interpreted via the Helmholtz condition in terms of $\gamma(\xi)$, then the expression for lift given above reduces to that given by Karman-Sears (Reference 8),

$$L' = \underbrace{-\rho \frac{d}{dt} \int_{-2b}^{+2b} \gamma_Q x dx}_{L'_a} + \underbrace{\rho V_\infty \Gamma_Q}_{L'_Q} + \underbrace{\rho V_\infty \int_{2b}^{\infty} \frac{\gamma(\xi)d\xi}{\sqrt{\left(\frac{\xi}{2b}\right)^2 - 1}}}_{L'_w} \quad . \qquad (1)$$

$\gamma_Q(x)$ is the quasi-steady vorticity distribution needed to make the airfoil a streamline (Kutta condition satisfied, but wake absent).

The apparent mass lift L'_a and quasi-steady lift L'_Q are easily computed from stationary thin airfoil theory. The wake lift requires special consideration. The method for obtaining each component of the lift is briefly outlined in the following paragraphs.

QUASI-STEADY LIFT L'_Q

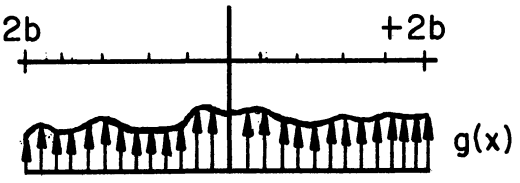

Fig. 7. Arbitrary distribution of normal velocity of an airfoil.

Let $g(x)$ be an arbitrary distribution of normal velocity over the airfoil as shown in Fig. 7. Then the quasi-steady circulation Γ_Q is

$$\Gamma_Q = 2\pi b \sum_{n=1}^{\infty} \frac{nB_n}{b^{n+1}} \qquad (2)$$

where

$$\frac{n\,B_n}{b^{n+1}} = \frac{2}{\pi} \int_{-\pi}^{\pi} g(x) \sin n\theta \quad \text{Sin } \theta \quad d\theta \qquad (2A)$$

with

$$x = 2b \text{ Cos } \theta \quad .$$

APPARENT MASS LIFT L'_a

To form this integral, γ_Q is needed.

$$\gamma_Q = \sum_{n=1}^{\infty} \frac{n\, B_n}{b^{n+1}} \left\{ \frac{1-\cos n\theta}{\sin \theta} \right\} \tag{3}$$

where the coefficient is given by (2A) above.

WAKE LIFT L'_w

The wake lift is found in terms of Γ_Q by first finding the L'_w following a unit jump in Γ_Q (Wagner Problem). The wake lift for a continuously varying Γ_Q is then found by linear superposition (Duhamel Integration).

The vorticity distribution in the wake following a unit jump in Γ_Q was found by Wagner. Using this $\gamma(\xi)$ in the last term of Eq. 1, Karman-Sears and others were able to express L'_w as follows:

$$L'_w(\sigma) = -\rho V_\infty \Phi(\sigma) \quad , \tag{4}$$

where σ is the nondimensional time $V_\infty t/2b$ and represents the half chords of travel following the unit jump in Γ_q. Jones fitted the following formula to the numerical values of $\Phi(\sigma)$.

$$\Phi(\sigma) = 0.165e^{-0.0455\sigma} + 0.335e^{-0.300\sigma} \quad . \tag{5}$$

By applying the superposition integral to the lift, Eq. 4, generated by a unit jump in Γ_Q, we find the wake lift L'_w at any time σ following the start of a continuously varying Γ_Q.

$$L'_w(\sigma) = -\rho V_\infty \int_0^\sigma \dot{\Gamma}_q(\nu)\Phi(\sigma-\nu)d\nu = -\rho V_\infty \left\{ \dot{\Gamma}_q * \Phi \right\} \tag{6}$$

where $$\dot{\Gamma}_q = \frac{\partial \Gamma_q}{\partial \sigma} \quad .$$

The information in this section is sufficient to compute the lift lag following an arbitrary time variation in the chordwise local angle of attack distribution.

TEST RESULTS ON THE MOVING BUMP GENERATOR

Quasi-steady and dynamic measurements of the lift and hot-wire measurements of the flow pattern were obtained in the manner described in References 32, 33, and 34 for a pilot model of the moving-bump gust generator.

The quasi-steady lift force as measured in the manner described in Reference 34

is not the true quasi-steady lift. The uncorrected quasi-steady lift is determined by placing the bump in a series of static positions. When the bump moves, however, the gust profile is modified, due to the motion of the bump. The true quasi-steady lift is found by taking the product of the uncorrected quasi-steady lift and the ratio of the difference between the free stream velocity and the bump velocity, and the free stream velocity.

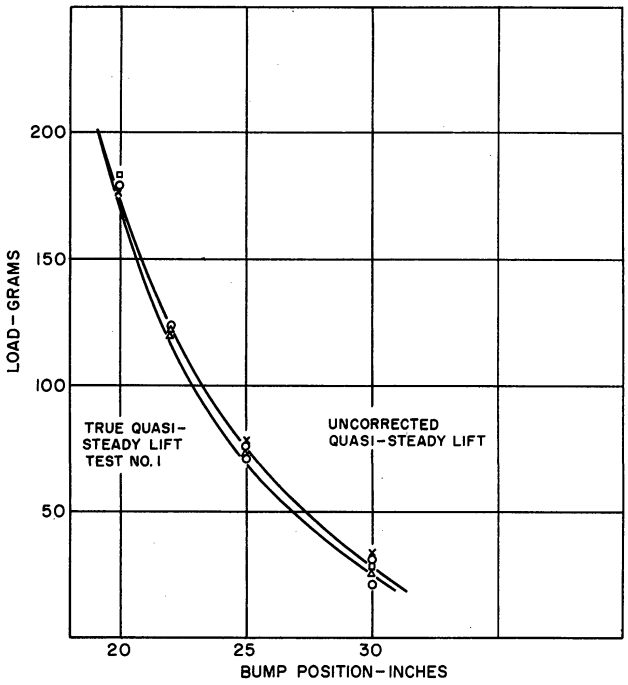

Fig. 8. Quasi-steady lift force vs bump position.

Figure 8 shows the uncorrected quasi-steady lift force as a function of bump position for a constant tunnel speed. Five runs were taken under similar conditions. A curve has been drawn through the arithmetic mean of the test data, and the scatter is interpreted as an uncertainty. The true quasi-steady lift was determined by the manner described above.

Figures 9 through 12 show the dynamic tests. Each of these figures represents a series of runs at a particular shock-cord tension. The range of bump speeds for each run is indicated on the figure. All tests were conducted at constant tunnel speed of 40 feet per second. The lift of the airfoil and bump position are plotted versus time in these curves. The plot of bump position versus time has been compensated to take into account a shift in the zero reference.

Figure 13 shows a cross plot of lift versus bump position of the dynamic runs taken from the curves of Figs. 9 through 12. The uncorrected quasi-steady plot of lift versus bump position is taken from Fig. 8.

The difference between the true quasi-steady and dynamic responses is represented in Fig. 14 as lift lag versus bump position. In Fig. 15 the lift lag versus time is presented. In these figures only data from the first test is plotted.

Figure 16 shows the measured values of flow deflection as a function of bump position for quasi-steady and dynamic flow using hot-wire, and quasi-steady flow measured by means of the pressure probe.

The scatter of the experimental points in Figs. 9 through 13 and Fig. 16 were caused largely by unsteadiness in the wind-tunnel airstream. As used for these tests, the tunnel had a relatively high turbulence level and, in addition, there were low period excursions from the mean velocity, probably caused by movement of the flow separation point in the diffusor.* Consequently, the results shown in Figs. 14 and 15 show an r.m.s. deviation of 3 grams in lift response.

*Since the tests reported here were completed, the 20- x 30-ft tunnel has been overhauled, reducing the turbulence level to below 0.03 percent. Subsequent tests will utilize this improved airstream.

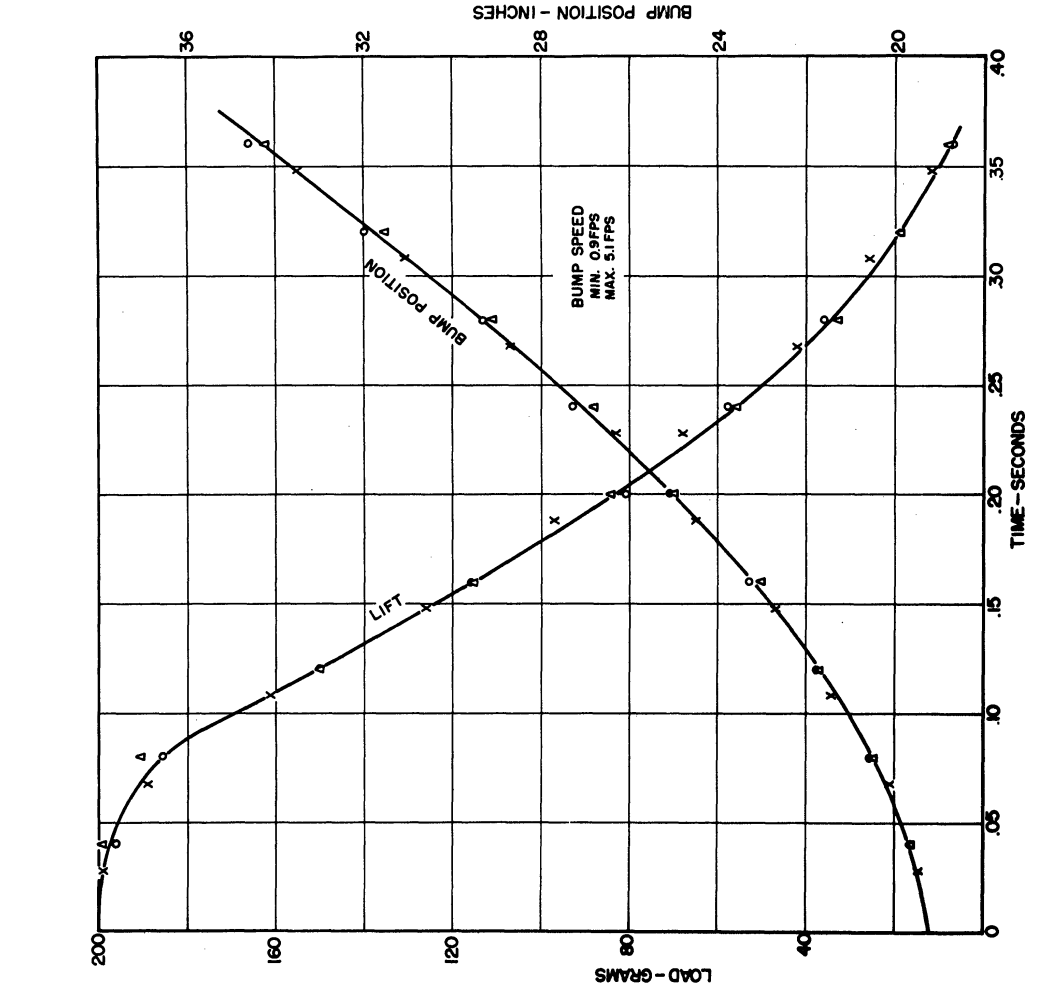

Fig. 10. Airfoil lift and bump position vs time for dynamic test No. 2 (Fig. 8 of Progress Report No. 3).

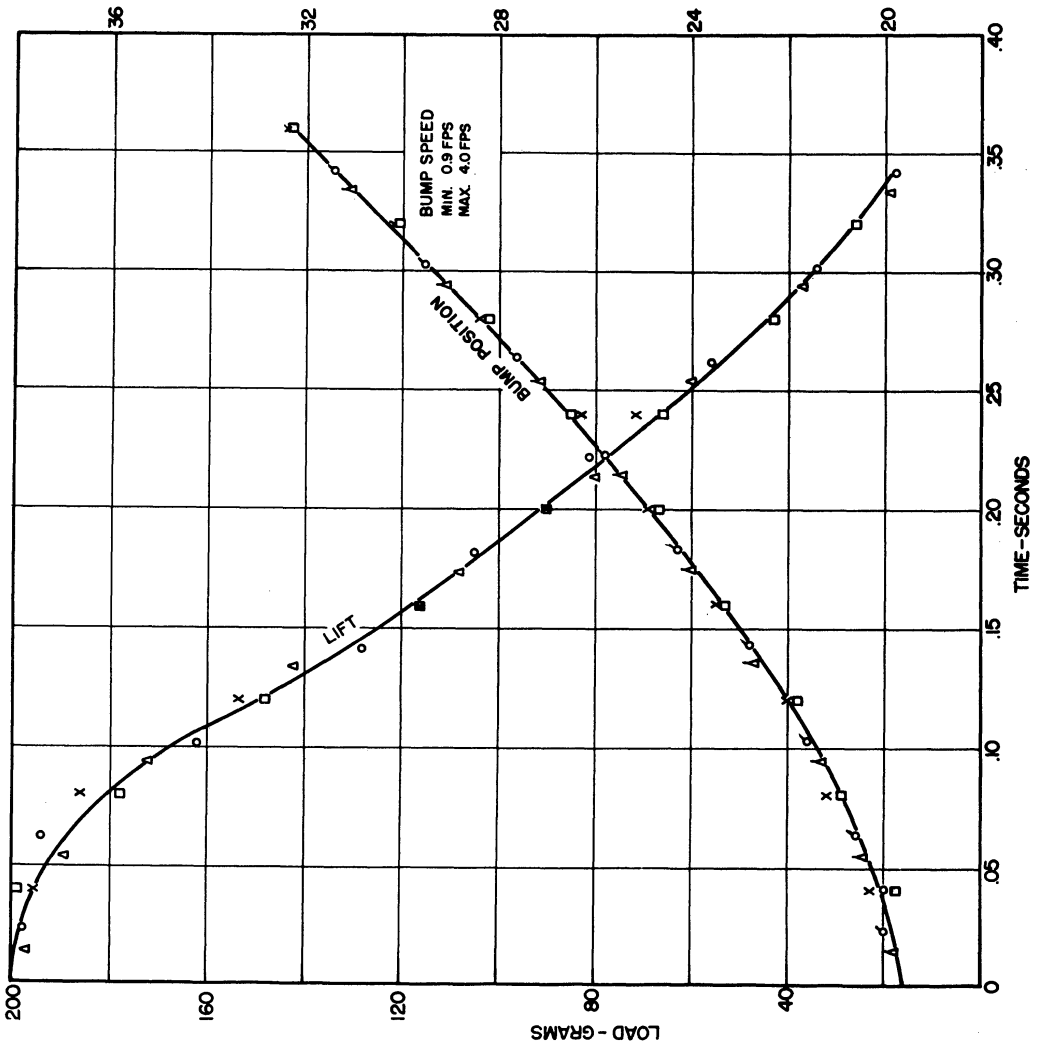

Fig. 9. Airfoil lift and bump position vs time for dynamic test No. 1 (Fig. 7 of Progress Report No. 3).

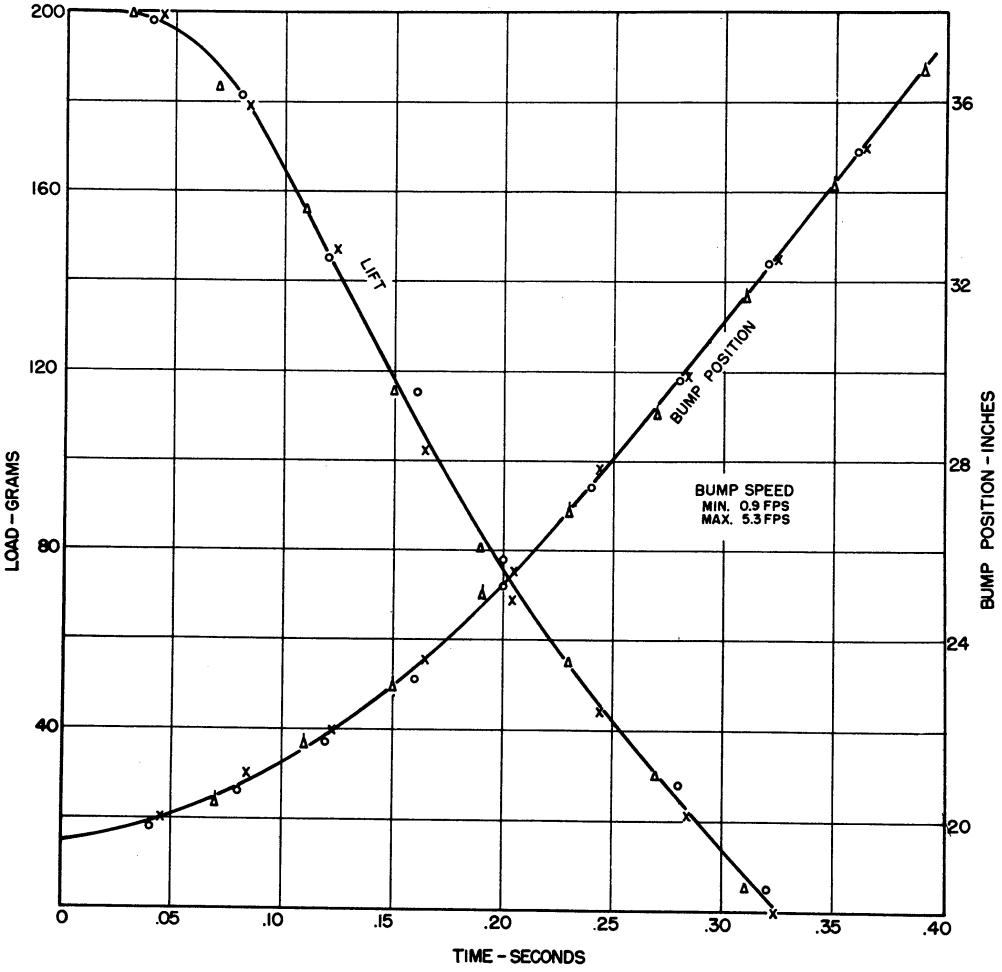

Fig. 11. Airfoil lift and bump position vs time for dynamic test No. 3 (Fig. 9 of Progress Report No. 3).

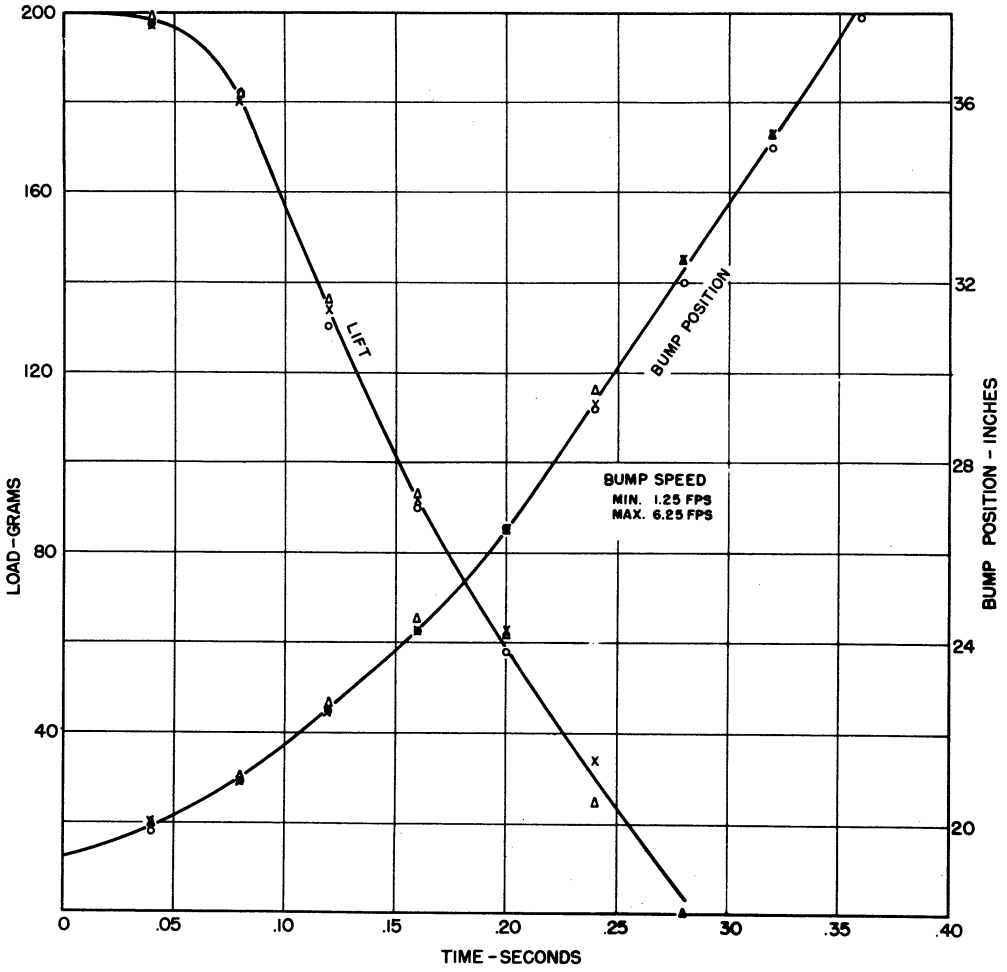

Fig. 12. Airfoil lift and bump position vs time for dynamic test No. 4 (Fig. 10 of Progress Report No. 3).

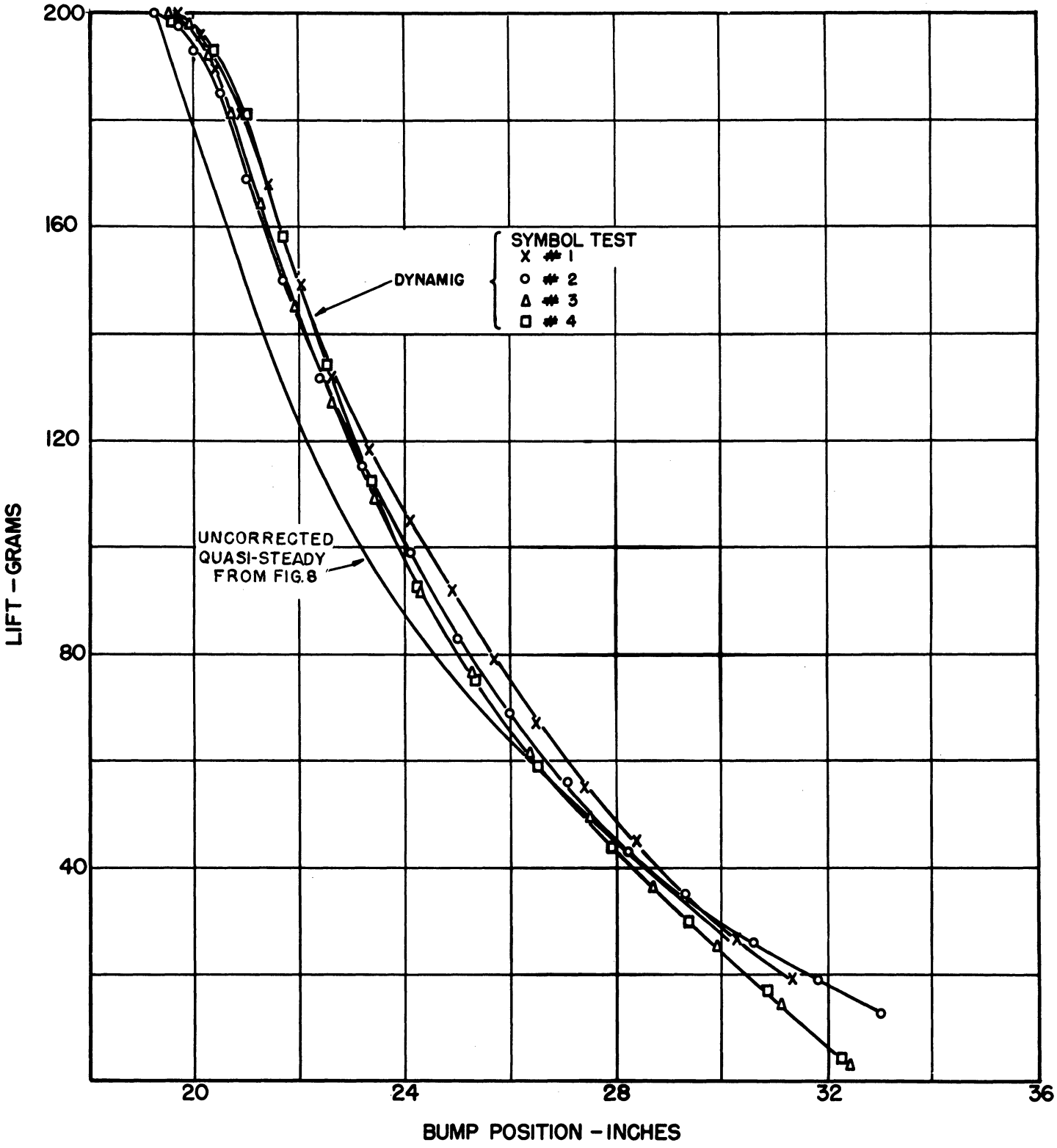

Fig. 13. Comparison of airfoil lift vs bump position for the dynamic tests and quasi-steady test (Fig. 11 of Progress Report No. 3).

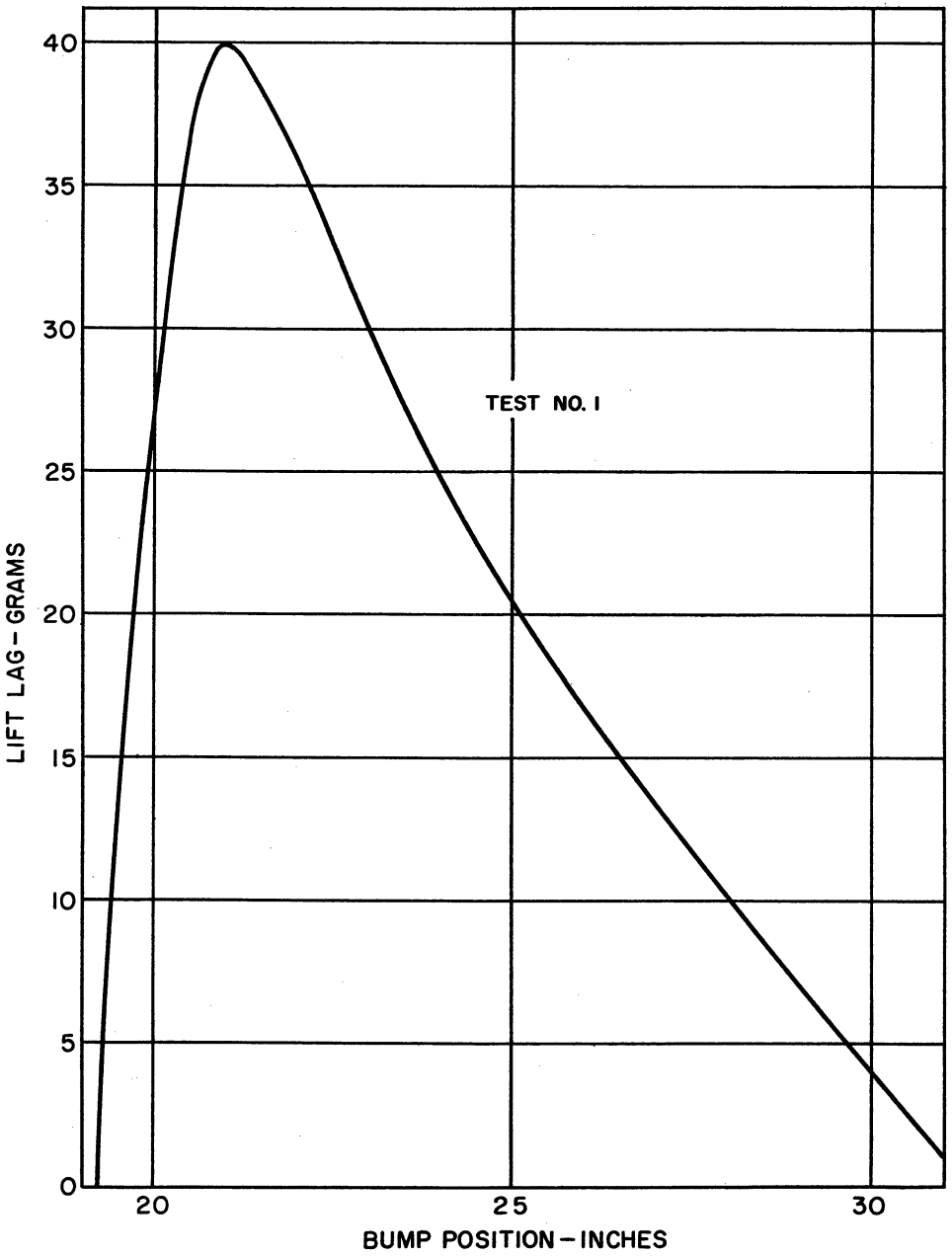

Fig. 14. Airfoil lift lag vs bump position, where lift lag = [dynamic lift - quasi-steady lift at the same bump position] .

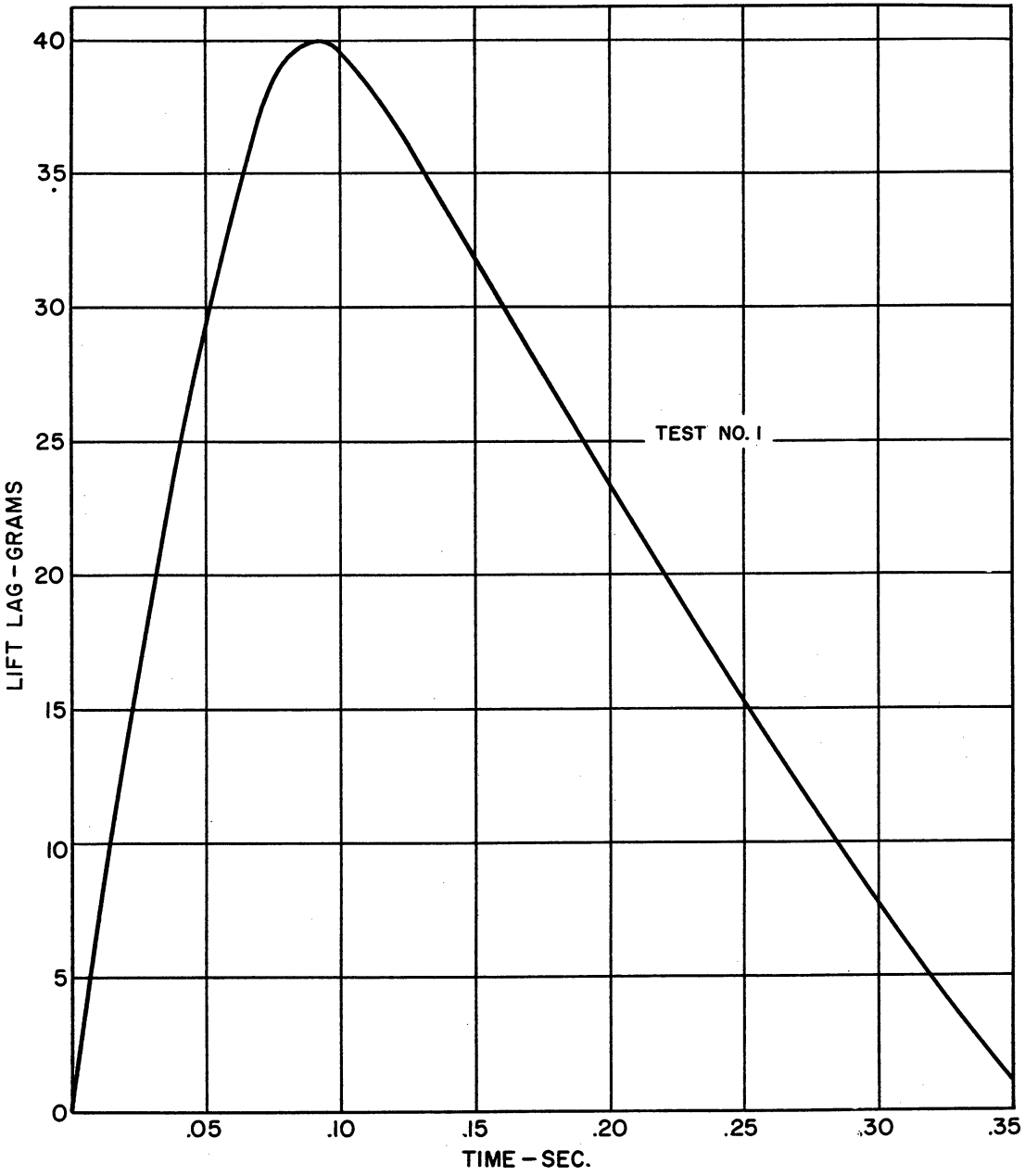

Fig. 15. Airfoil lift lag vs time.

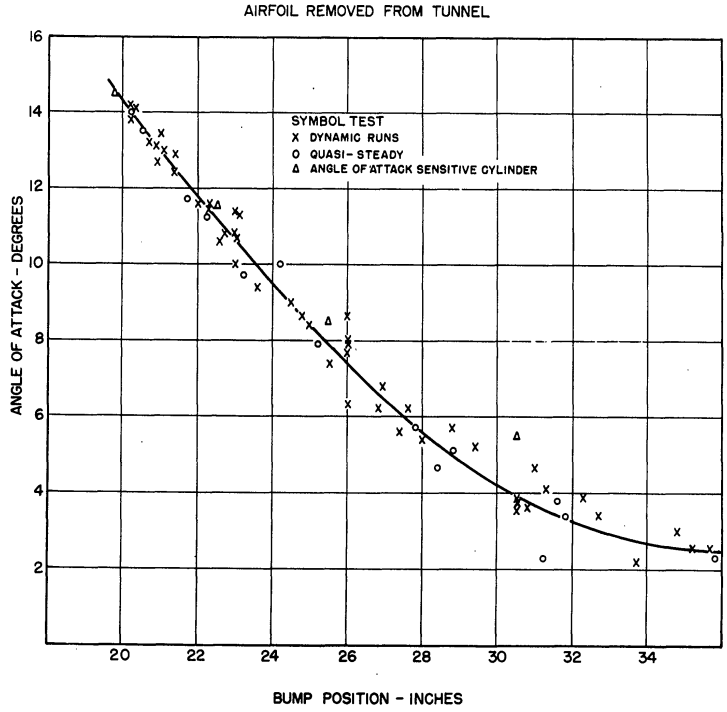

Fig. 16. Angle of flow deflection vs bump position at trailing edge position of airfoil (Fig. 14 of Progress Report No. 3).

In Fig. 16 the angle of flow deflection at the position of the airfoil trailing edge (with airfoil absent) is plotted for the range of bump positions. Test data were taken for both quasi-steady and dynamic conditions. The curves have been adjusted to agree at the forward bump position in order to eliminate zero shift errors. The average uncertainty in angle of attack is $\pm$ 0.35° from the faired curve of Fig. 16.

The local angle of attack variation with bump position as given by Fig. 16 was used in conjunction with the theory described earlier to compute the lift lag. The maximum lift lag predicted by theory is 39 grams. This compares with the experimental value of 40 grams shown in Figs. 14 and 15. The time at which the maximum occurs is approximately the same from theory and experiment.

The experiment has been compared with theory in order to get a rough quantitative estimate of the effectiveness of the gust-generating device and the measuring apparatus. It is pointed out that the theory has not been applied in the most accurate fashion possible, taking into account small variations in bump speed and tunnel wall interference effects. These refinements were considered unnecessary for present purposes.

The comparison between experiment and theory indicates that non-stationary flow effects are being generated and can be successfully measured.

TEST RESULTS ON THE VORTEX GENERATOR

Because there is no way of making the flow pattern stand still with the Vortex Generator gust-similating device, quasi-steady values of the lift cannot be obtained. As described in References 35 and 36, the flow pattern and dynamic lift are measured

simultaneously for each run. This makes repeatability unnecessary.

Tests were made at wind speeds of 15, 30, and 60 feet per second. Shown in Fig. 17 are the oscillograms for the above tunnel speed conditions. In Figs. 18a, 18b, and 18c are shown the reduced data for these tunnel speeds.

In Fig. 18a are shown 6 runs at a tunnel speed of 59.7 feet per second. The variations in lift measurements follow the variations in flow as shown by the monitor wire.

The hot-wire probe is located 2-1/2 inches ahead of the leading edge of the airfoil. Velocity measurements made at this station indicate that the same velocity occurs there as occurs at the reference pitot tube point for the tunnel. Thus, for a tunnel velocity of 59.7, 0.00350 seconds are required for the flow pattern to travel from the probe to the leading edge of the lifting surface. Similarly, it requires 0.0119 seconds for the pattern to travel from the probe to the trailing edge of the lifting surface. Referring to 18a, it can be observed that zero angle of attack as measured by the probe, and zero lift as measured by the balance are separated by an interval of approximately .025 seconds. Thus, there is a time delay of 0.013 to 0.021 seconds, which may be attributed to unsteady aerodynamics and balance response. Of this, not more than .004 seconds can be assigned to balance lag.

The maximum dynamic lift predicted by theory is about twice the experimental value shown in Fig. 18a. Whether the theory is incorrect for velocity gradients of the magnitude indicated here, or the instrumentation is inadequate, is uncertain until an accurate balance calibration is completed.

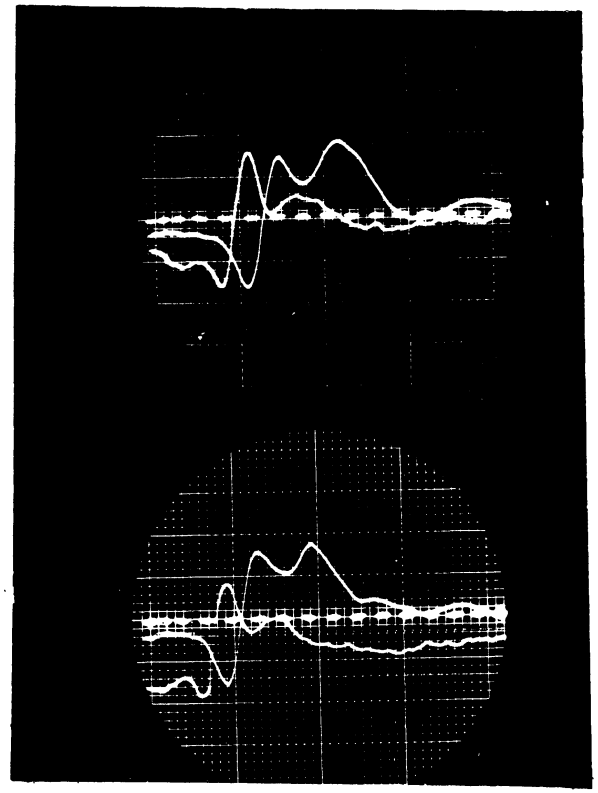

a

Tunnel speed = 59.7 ft/sec.
Dashed line is a 50-cps time pulse.
Monitor probe trace is first trace to cross time-pulse line in both pictures.
Lifting surface trace is second trace to cross time-pulse line in both pictures.

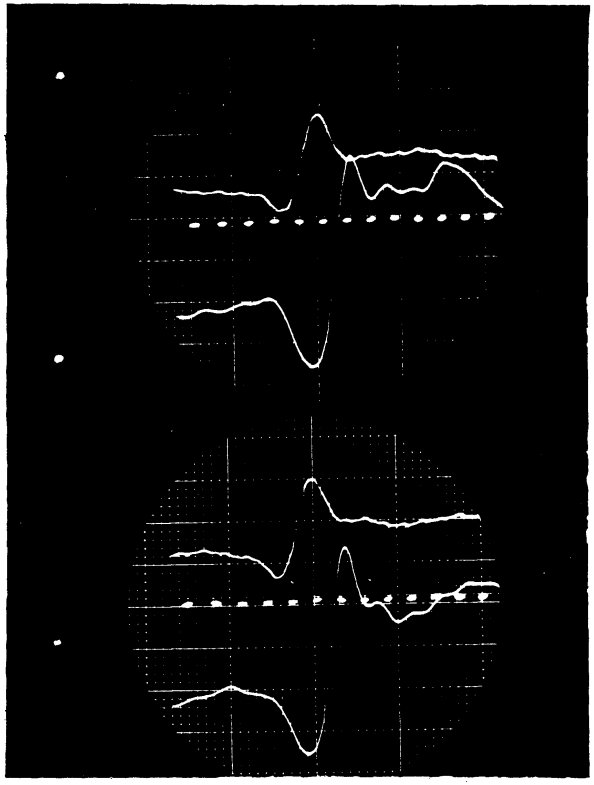

b

Tunnel speed = 30 ft/sec.
Dashed line is a 50-cps time pulse.
Monitor probe is upper trace in both pictures.
Lifting surface response is lower curve in both pictures.

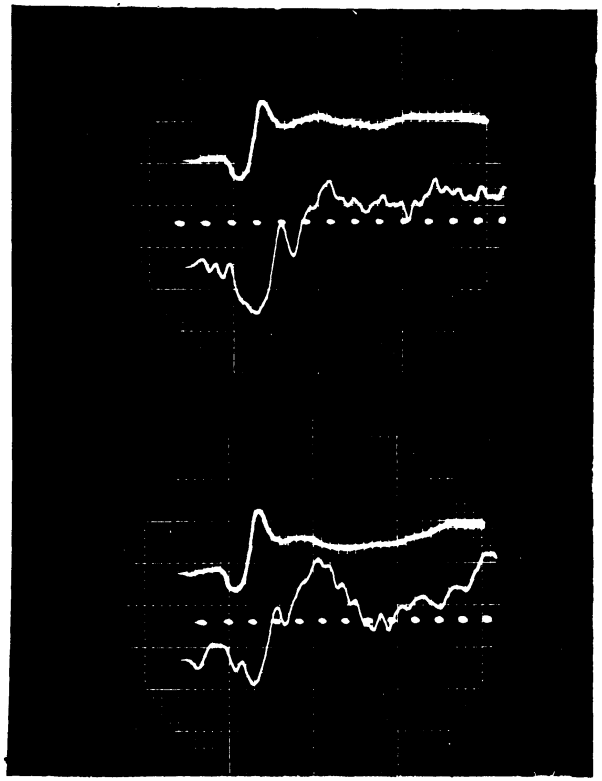

c

Tunnel speed = 15 ft/sec.
Dashed line is a 50-cps time pulse.
Monitor probe is upper curve in both pictures.
Lifting-surface response is lower curve in both pictures.

Fig. 17. Oscillograms of the lifting-surface and monitor-probe responses to the vortex generator. (Fig. 9 of Progress Report No. 5).

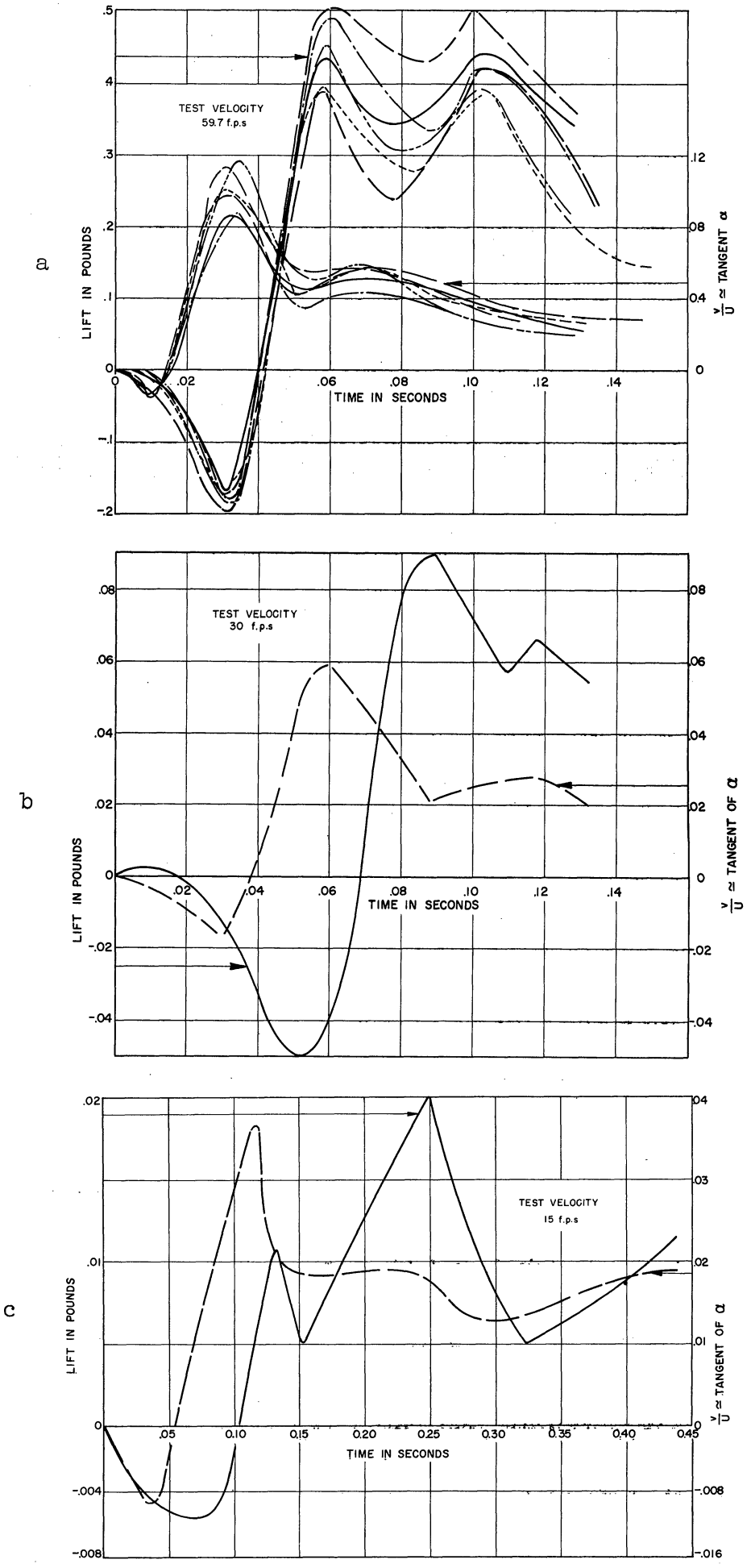

Fig. 18. Responses of lifting surface and monitor probe to vortex generator (Figs. 10a, 10b, and 10c of Progress Report No. 5).

MODEL GUST GENERATOR

With the present gust-generation model it is possible to test to Reynolds' numbers of 130,000 with an airfoil of six inches. This Reynolds' number is too low to assess accurately the operation of either the gust-generating devices or the instrumentation. Therefore, it is necessary to build a larger model.

In Fig. 19 is shown an artist's sketch of the circuit and in Fig. 20 is shown the plan view of the system.

The model is being constructed on University of Michigan property, the cost of Stations 5 through 13 (see Fig. 20) and of the building housing the test section to be borne by the University, while the cost of that portion from Stations 13 through the working section to Station 5 is chargeable to the contract, since it has been designed with special attention to the problem of gust simulation and to the achievement of low turbulence.

Important items in the configuration and performance are listed below:

A. Basic Dimensions

Test Section

Width - 7 ft
Height - 5 ft
Length - 25 ft

Settling Chamber

Contraction ratio - 15
Width - 26 ft
Height - 20 ft
Length - 20 ft
Number of screens in settling chamber - 5

First Diffuser

Equivalent cone angle
Section (2-3) - 3°
Section (3-4) - 5°

Area ratio: test section area/area at Station 4 - 0.224

Length of diffuser - 44 ft

B. Aerodynamic Performance in Test Section

Speed range - zero to 230 ft/sec at a test-section density of one atmosphere.

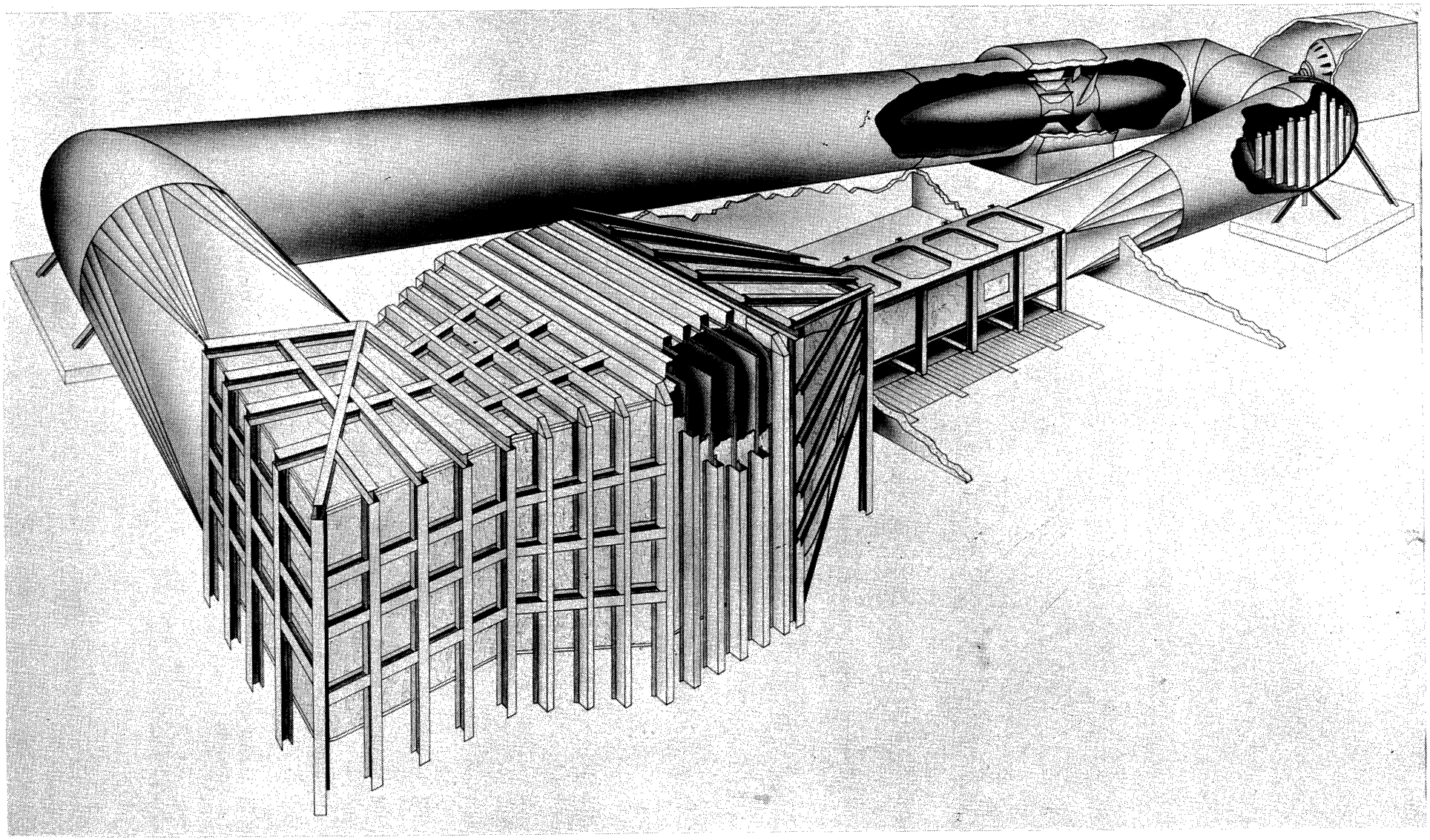

Fig. 19. Perspective drawing of gust-generator model. (Fig. 11 of Progress Report No. 5).

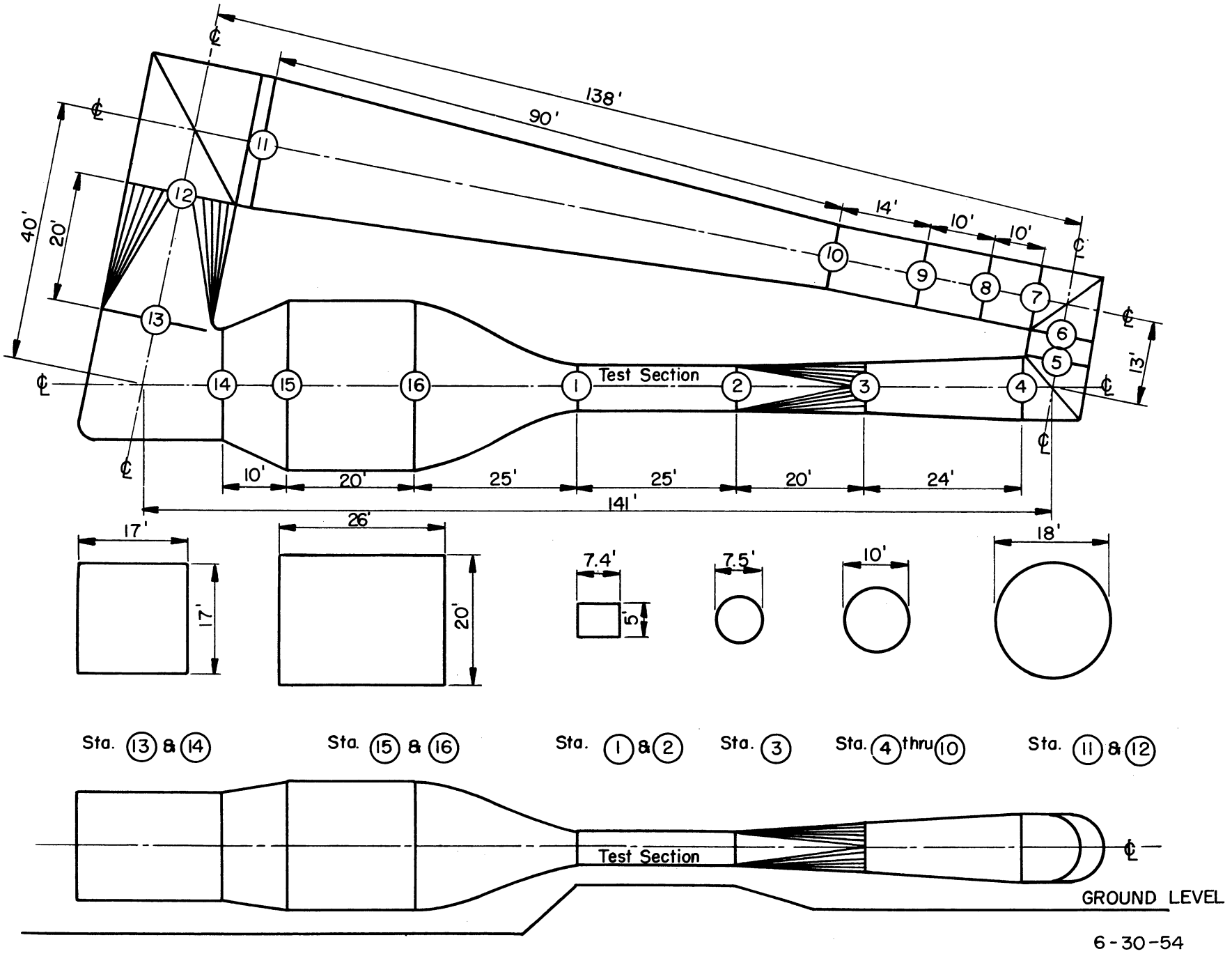

Fig. 20. Plan view of gust-generator model (Fig. 12 of Progress Report No. 5).

Maximum Reynolds' number - 1.5×10^6 per ft for a density of one atmosphere in the test section.

Free stream turbulence - 0.01%

C. Gust Simulation Device

A gust generator of the "moving bump" type will be built and installed in the test section.

D. Power Requirements and Power Plant

The power plant will be of the Ward-Leonard type system and will be capable of developing 1000 horsepower. The fan has been designed by methods outlined in Reference 37. The fan will have 10 blades and there will be 7 straightener vanes; details are given in References 38 and 39.

A power factor of 0.30 is calculated for the circuit. Thus, at a test section speed of 230 ft/sec, the power required is 280 horsepower. Tabulated below is a breakdown of the contribution of the various circuit components to the total power factor. See Fig. 20 for station locations.

1. Wall Friction Losses

a. test section	0.0395	
b. settling chamber	.00004	
c. nozzle section	.0032	
d. fan section	.0176	
		0.0603

2. Diffuser Losses

Section (2-3)	0.0590	
Section (3-4)	.0519	
Section (10-11)	.0218	
Section (12-13)	.0007	
		.1334

3. Rapid Expansion Section .0061

4. Corner Losses

Corner (4-5)	0.0280	
Corner (6-7)	.0280	
Corner (11-12)	.0028	
Corner (13-14)	.0022	
		.0610

5. Screen Losses .0450

Total value for power factor 0.3000

Details of the above results are given in Reference 40.

SIGNIFICANT RESULTS AND WORK IN PROGRESS

The sample results given in Fig. 16 indicate the feasibility of simulating gusts in wind tunnels. The airstream in which these tests were made was quite turbulent and the Reynolds' number was quite low (130,000). The later work with the pilot model tunnel will be directed toward refinement of the equipment to make it applicable for tests in the 5- x 7-ft working section now under contract.

Dynamic calibrations of the lift balance are being carried out. One of the greatest difficulties in these calibrations is the method of application of the fluctuating load. If the area over which the load is applied to the wing is too small, local deflections will introduce a lag which is a function of the details of the calibration method. The first wing model was covered with thin balsa sheet and the difficulty described was encountered. A new wing is currently being constructed with a sheet metal skin; the load will be applied through a sleeve which fits closely over the wing.

Some consideration is being given to the use of pressure capsules to measure pressure distributions on wings and bodies in unsteady flow. The actual taking of data would be more difficult than with a balance system, but the response of the pressure capsule is not affected by the inertia of the model and, therefore, higher frequency contributions to forces and moments can be detected.

In connection with the discrepancy between theory and experiments on the vortex generator device, some experiments will be initiated to determine whether the Kutta condition is continuously satisfied throughout a rapid change in flow direction.

The 5- x 7-ft wind tunnel has been contracted for with the Nooter Corporation of St. Louis. Construction will begin in the spring and should be completed early in the fall of 1955. Every effort will be made to reduce the turbulence to a very low value so that the utility of the airstream will extend to tests in which low turbulence is of paramount importance.

Design of the working section and gust-simulation equipment will be finished by early summer so that construction will be completed simultaneously with the rest of the equipment and buildings.

REFERENCES

1. Donely, P. An Experimental Investigation of the Normal Acceleration of an Airplane Model in a Gust. NACA TN 706.

2. Donely, P. Summary of Information Relating to Gust Loads on Airplanes. NACA TN 1976.

3. Bratt, J. B. and Scruton, C. Measurements of Pitching Moment Derivatives for an Airfoil Oscillating About the Half Chord Axis. Br ARC RAM. 1921.

4. Ashley, Zartarian, and Neilson. Investigation of Certain Unsteady Aerodynamic Effects in Longitudinal Dynamic Stability. MSAF TR 5986.

5. Buchan, Harris, and Summervail. Measurements of Z w for an Oscillating Airfoil. College of Aeronautics. Cranfield Report No. 40.

6. Halfman, R. L. Experimental Aerodynamic Derivatives of a Sinusoidally Oscillating Airfoil in Two-Dimensional Flow. NACA TN 2465.

7. Theodoisen, T. General Theory of Aerodynamic Instability and the Mechanism of Flutter. NACA TR 496.

8. Karman and Sears. Airfoil Theory for Non-Uniform Motion. J Aero Sci. August 1938.

9. Jones, R. T. The Unsteady Lift of a Finite Wing. NACA TR 681.

10. Luke, Y. L. Table of Coefficients for Compressible Flutter Calculations. USAF TR 6800.

11. Mazelsky, B. Determination of Indicial Lift and Moment of a Two-Dimensional Pitching Airfoil at Subsonic Mech Numbers from Oscillating Coefficients with Numerical Calculations for M = 0.7. NACA TN 2613.

12. Brat, M. A. Loads on a Supersonic Wing Striking a Sharp Edged Gust. J Aero Sci. May 1949.

13. Garrick and Rubinow. Theoretical Study of Air Forces on an Oscillating or Steady Thin Wing in a Supersonic Main Stream. NACA TN 1383.

14. Reissmer, E. Effect of Finite Span on the Airload Distribution for Oscillating Wings. NACA TN 1194, TN 1195.

15. Brat and Boehnlein. Aerodynamic Theory of Oscillating Wings of Finite Span. Galcit Report No. 5.

16. Wasserman, S. Aspect Ratio Corrections in Flutter Calculations. USAF MR MCREXA 5-4595-8-5.

17. Walker, P. B. Growth of Circulation About a Wing and Apparatus for Measuring Fluid Motion. Br ARC RsM 1402.

18. Farren, W. S. Reaction on a Wing Whose Angle of Incidence is Changing Rapidly. Br ARC RsM 1648.

19. Kuethe, A. M. Circulation Measurements About the Tip of an Airfoil During Flight Through a Gust. NACA TN 685.

20. Bisplinghoff, Isakson, and O'Brien. Gust Loads on a Rigid Airplane with Pitching Neglected. J Aero Sci. January 1951.

21. Kordes and Hanbolt. Evaluation of Gust Response Characteristics of Some Existing Aircraft with Wing Bending Flexibility Included. NACA TN 2897.

22. Goland, M., et al. Effects of Airplane Elasticity and Unsteady Flow on Longitudinal Stability. Midwest Research Institute Project No. R108E-108.

23. Statler, I. C. Dynamic Stability at High Speed from Unsteady Flow Theory. J Aero Sci. April 1950.

24. Lyon and Ripley. A General Survey of the Effects of Flexibility of the Fuselage, Tail Unit, and Control Systems on Longitudinal Stability and Control. Br ARC RsM 2415.

25. Pai and Sears. Some Aeroelastic Properties of Swept Wings. J Aero Sci. February 1949.

26. Schetzer, J. D. Dynamics for Aerodynamicists. Douglas Aircraft Company. S M 14077.

27. Donely, P. Effective Gust Structure at Low Altitude as Determined from the Reactions of an Airplane. NACA TR 692.

28. Clementson, G. An Investigation of the Power Spectral Density of Atmospheric Turbulence. MIT. Thesis, 1950.

29. Sherlock, R. H. Storm Loading and Strength of Wood Pole Lines and Study of Wind Gusts. Edison Electric Institute. 1936.

30. Br RAE Report, Aero 2341. High Altitude Gust Investigation.

31. Huss and Portman. Study of Natural Winds and Computation of the Austausch Turbulence Constant. Guggenheim Airship Institute. Report No. 149.

32. University of Michigan, Engineering Research Institute. Progress Report No. 1, Project 2099.

33. University of Michigan, Engineering Research Institute. Progress Report No. 2, Project 2099.

34. University of Michigan, Engineering Research Institute. Research Design Problems Relating to Facilities for Simulating the Aerodynamic Effects of Atmospheric Gusts on Aircraft Components. Progress Report No. 3.

35. University of Michigan, Engineering Research Institute. Research Design Problems Relating to Facilities for Simulating the Aerodynamic Effects of Atmospheric Gusts on Aircraft Components. Progress Report No. 4.

36. University of Michigan, Engineering Research Institute. Research Design Problems Relating to Facilities for Simulating the Aerodynamic Effects of Atmospheric Gusts on Aircraft Components. Progress Report No. 5.

37. Patterson, G. N. Ducted Fans: Design for High Efficiency. ACA 7. 1944.

38. Roensch, R. L. A Method for Determining the Design Specifications for a Fan-Strengthener Configuration. University of Michigan, Department of Aeronautical Engineering. Project 2099 - GTM 6. July 1954.

39. Roensch, R. L. Fan-Strengthener Design for Gust Generator Model. University of Michigan, Department of Aeronautical Engineering. Project 2099 - GTM 8.

40. Garby, L. C., Raman, K. R., and Roensch, R. L. Estimation of the Power Factor for the 5- x 7-ft Tunnel. University of Michigan, Department of Aeronautical Engineering. Project 2099 - GTM 4.